Computer Modeling of Lithium Phosphate and Thiophosphate Electrolyte Materials

N. A. W. Holzwarth, Nicholas Lepley and Yaojun A. Du[a]

Department of Physics, Wake Forest University, Winston-Salem, NC, USA

[a]Current address: ICAMS, Ruhr-Universität, 44780 Bochum, Germany

Introduction

Lithium phosphorous oxynitride (LiPON) films were developed at Oak Ridge National Laboratory[1] as very promising solid state electrolytes for use in rechargeable batteries and other applications. The films have compositions close to that of crystalline Li_3PO_4 and ionic conductivities of 10^{-6} S/cm. In previous work,[2] we investigated detailed mechanisms for Li ion migration in idealized models of LiPON based on Li_3PO_4 and related phosphonitrides. In those materials we found that Li ions can diffuse by vacancy and interstitial mechanisms with migration energies of 0.3-0.7 eV. In the present work, we report preliminary results for extending this modeling study to lithium thiophosphate materials which have recently received attention as promising candidates for solid-state electrolytes[3] where increased ionic conductivity as large as 10^{-3} S/cm has been reported.

In this work, several lithium phosphate and thiophosphate materials are modeled to determine their optimized lattice structures, their total energies, and their electronic structures. Included in this study are materials characterized by isolated phosphate and thiophosphate groups – Li_3PS_4 and Li_3PO_4 and materials characterized by phosphate and thiophosphate dimers – $Li_4P_2S_6$ and $Li_4P_2O_6$ and $Li_4P_2S_7$ and $Li_4P_2O_7$. In addition, the superionic conducting material $Li_7P_3S_{11}$ is also modeled as are recently discovered crystalline argyrodite materials Li_7PS_6 and Li_6PS_5Cl. A comparison of Li ion vacancy migration in $Li_4P_2S_7$ and $Li_4P_2O_7$ shows that the migration energy barrier to be smaller (less than one-half) in the thiophosphate material than in the phosphate material.

Calculational Methods

The computational methods used in this work were the same as those used in our previous studies of electrolytes related to LiPON. In Ref. [2], the choice of calculational parameters and the validation of the calculational methods are presented. Briefly, we used density functional theory[4] to treat the electronic states and the Born-Oppenheimer approximation to treat the atomic positions $\{\mathbf{R}^a\}$, resulting in a determination of the "total energy" $E(\{\mathbf{R}^a\})$ of the system. The local density approximation (LDA)[5] was used for the exchange-correlation functional. Most of the computations were carried out using the *PWscf* package;[6] while a few calculations were performed using the *abinit*[7] and *pwpaw*[8] packages as well. Visualizations were constructed using the *OpenDX*[9] and *XCrySDEN*[10] software packages.

Starting from experimental information for each material or a related material, restricted optimization of the total energy $E(\{\mathbf{R}^a\})$ with respect to the atomic positions $\{\mathbf{R}^a\}$ and unit cell parameters, allows us to model stable and meta-stable structures and to estimate the heat of formation (ΔH). For each meta-stable structure, a qualitative picture of the valence state distribution can be determined from the averaged partial densities of states $\langle N^a(E)\rangle$. In addition, migration energies (E_m) for Li ion migration were estimated using the "nudged elastic band" method.[11]

Li_3PS_4 and Li_3PO_4

Li_3PS_4 and Li_3PO_4 are characterized by isolated phosphate or thiophosphate groups. Li_3PO_4 has been reported in two different orthorhombic crystalline forms – the β form[12] has symmetry $Pmn2_1$ (#31) and the γ form[13] has symmetry $Pnma$ (#62). In our previous work we found that the β form is more stable by 0.03 eV per formula unit, while more experimental results are reported for the γ form. The crystal structure of Li_3PS_4 was reported by Mercier *et al.*[14] to have an orthorhombic symmetry $Pnma$ (#62) which differs from γ-Li_3PO_4 structure because of different site occupancies, some of which are fractional. We determined optimized total energies for Li_3PS_4 in several approximations to the Mercier structure and in the β and γ structures of Li_3PO_4, and found the lowest energy structure to be that of β-Li_3PO_4. Our results indicate this structure to be more stable than the most stable approximation to the Mercier structure by 0.1 eV per formula unit and more stable than the γ-Li_3PO_4 structure by 0.2 eV per formula unit. The comparison of Li_3PS_4 and Li_3PO_4 in the β-Li_3PO_4 is illustrated in Fig. 1. The lattice parameters of Li_3PS_4 are found to be roughly 25% larger than those of Li_3PO_4 and the fractional coordinates are quite similar for the two structures.

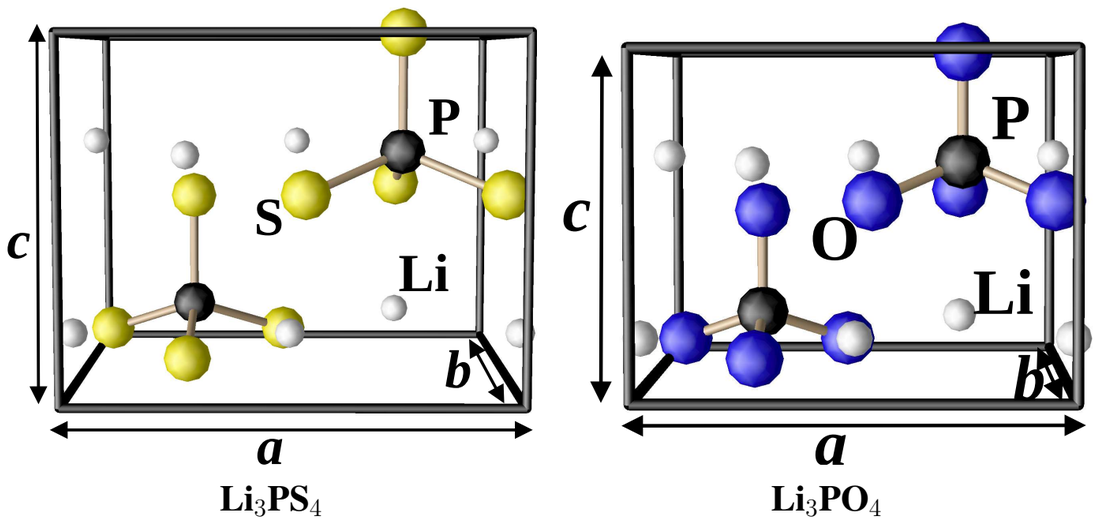

FIG. 1 Ball and stick diagrams for Li_3PS_4 and Li_3PO_4 in the $Pmn2_1$ structure (β-Li_3PO_4).

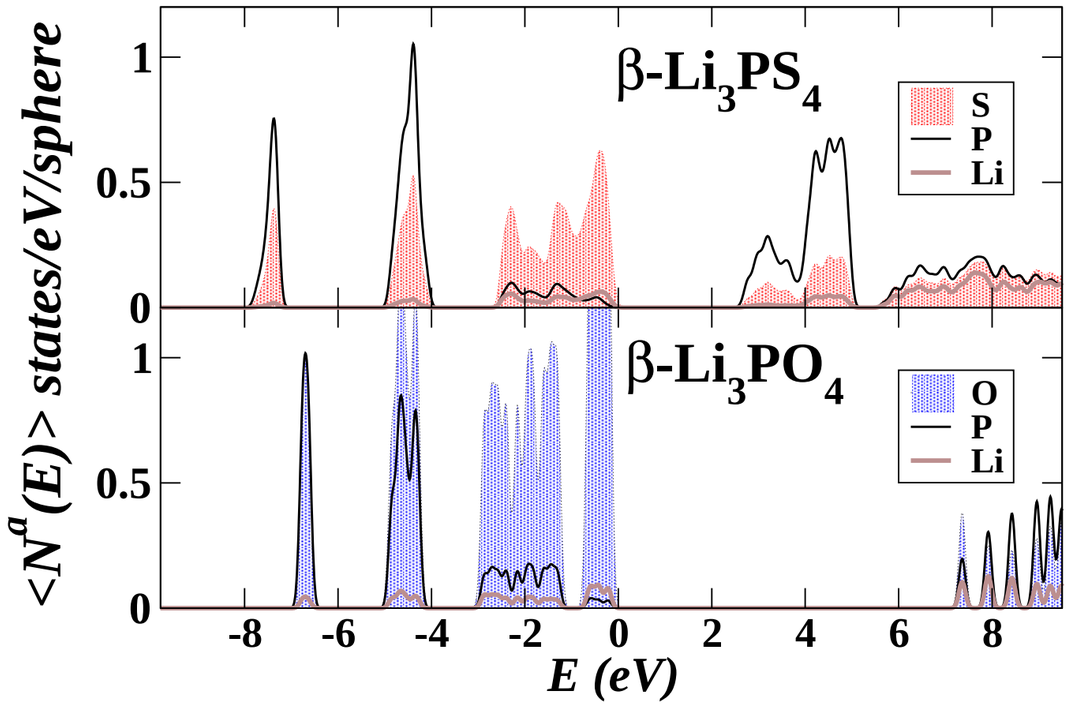

FIG.2 Partial densities of states for Li_3PS_4 and Li_3PO_4.

In Fig. 2 the partial densities of states of Li_3PS_4 and Li_3PO_4 are compared. The S $3p$ valence bands of Li_3PS_4 cover a wider range of energies than does the O $2p$ valence bands of Li_3PO_4. As noted in our earlier work the two lower bands have $p\sigma$ character with significant hybridization with the P $3s$ and $3p$ states, while the top of the valence band is has $p\pi$ character. It is interesting to note that the magnitudes of the O contributions to $\langle N^a(E)\rangle$ the partial densities of states are generally larger than those of S, indicating that the charge of the O $2p$ states is more confined within the analysis sphere than is the charge of the S $3p$ states. While the calculated band gaps within density functional theory are systematically underestimated, it is clear that the gap in Li_3PS_4 is less than half of that in Li_3PO_4.

Li_7PS_6 and Li_5PS_5Cl

There has been a number of recent studies of lithium thiophosphate materials with additional sulfur and lithium ions in a structure associated with the mineral argyrodite.[15] The high Li ion conductivity observed[16] in these materials is associated with high-temperature crystalline forms having multiple fractional occupancy sites. However, these materials also have ordered low-temperature structures which we have modeled in this work. The low temperature structure of Li_7PS_6 has been found to be $Pna2_1$ (#33). The low temperature structure of Li_6PS_5Cl has not been reported, but it is reasonable to assume that it is similar to that reported for Li_6PS_5I which forms a monoclinic structure with Cc (#9) symmetry. The calculations optimized the Li_7PS_6 and Li_6PS_5Cl structures and the results are illustrated in Fig. 4. For Li_7PS_6 there are two unbounded S ions associated with each thiophosphate group and for Li_6PS_5Cl there is one unbounded S ion and one unbounded Cl ion for each thiophosphate group.

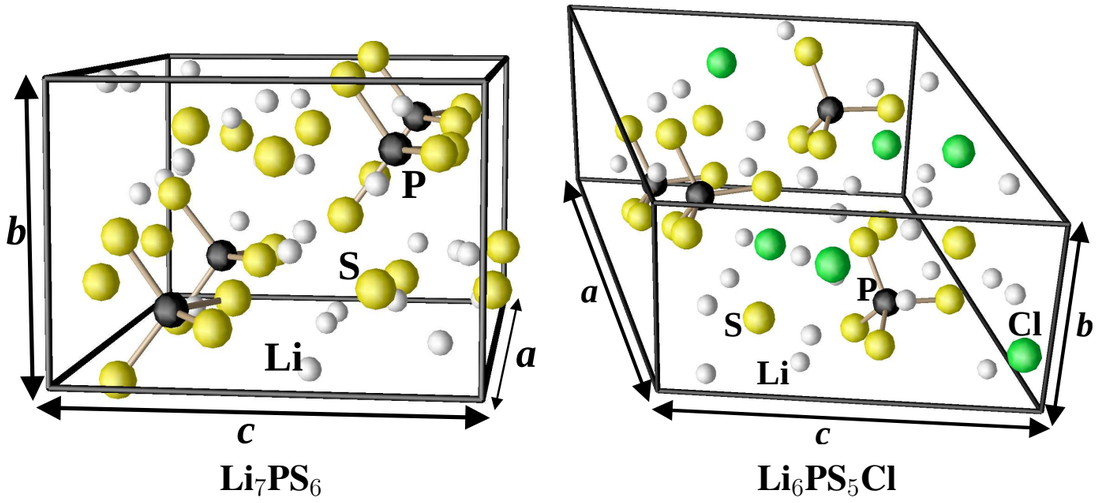

FIG. 3 Ball and stick diagrams for Li_7PS_6 in the $Pna2_1$ structure (left) and Li_6PS_5Cl in the Cc structure (right).

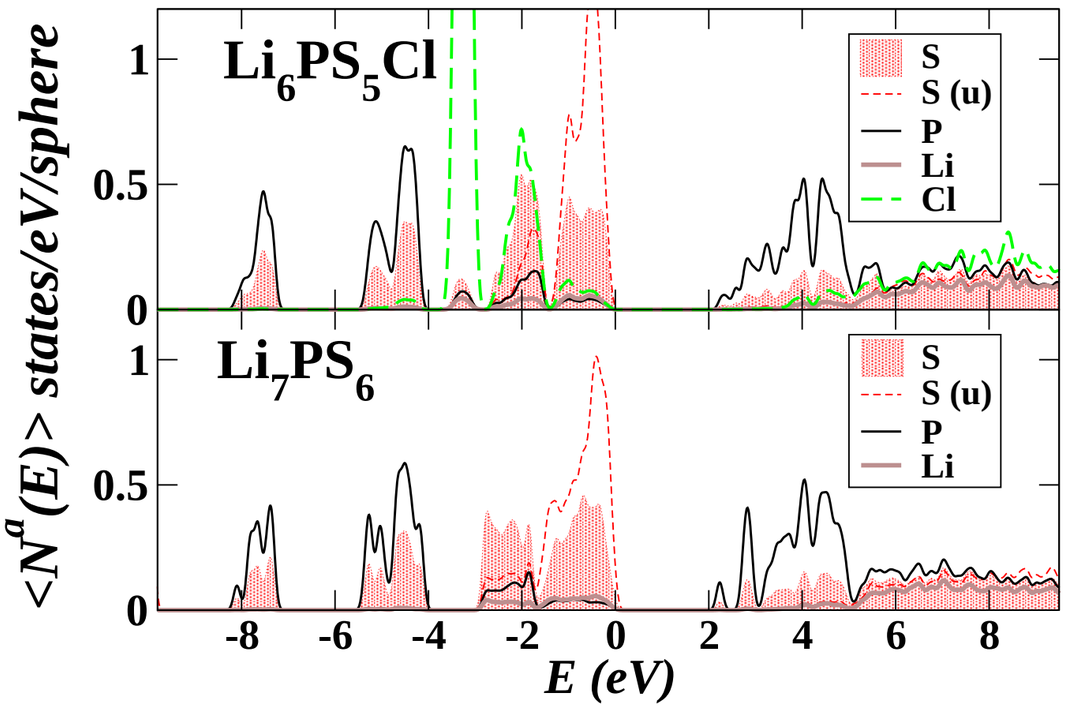

FIG.4 Partial densities of states for Li_7PS_6 and Li_6PS_5Cl. Contributions from unbounded S sites are indicated with "(u)".

Next we consider the partial densities of states of the argyrodite structured thiophosphates, comparing the partial densities of states of Li_7PS_6 and Li_6PS_5Cl in Fig. 4. For Li_7PS_6, the isolated S ions are found to contribute relatively narrow bands near the top of the valence band. For Li_6PS_5Cl, the isolated Cl ion con tributions are at lower energy than those of the isolated S ions.

$Li_4P_2S_6$ and $Li_4P_2O_6$

The crystal structure of $Li_4P_2S_6$ was described by Mercier[17] as hexagonal $P6_3/mcm$ (#193) with half occupancy of the P ($4e$) sites. Our electronic structure calculations of the 6 possible configurations of this unit cell find the lowest energy structure to be described by the $P\bar{3}1m$ (#162) structure which is a subgroup of the original space group. In this hexagonal group, the Li ions are located at $2c$ $(1/3, 2/3, 0)$ and $2d$ $(1/3, 2/3, 1/2)$ sites, the P ions are located at $2e$ $(0, 0, z_P)$ sites, and the S ions are located at $6k$ $(x_S, 0, z_S)$ sites. We were also able to simulate a meta-stable phosphate material – $Li_4P_2O_6$ – with the same structurer.

In constrast to the other phosphates and thiophosphates, an interesting characteristic of the optimized $Li_4P_2S_6$ and $Li_4P_2O_6$ structures is the presence of a direct bond between two P ions. In $Li_4P_2S_6$ the P-P bond length is 2.24 Å which is 10% longer than the P-S bond length, while in $Li_4P_2O_6$ the P-P bond length is 2.10 Å which is 40% longer than the P-O bond length. This is illustrated in Fig. 5.

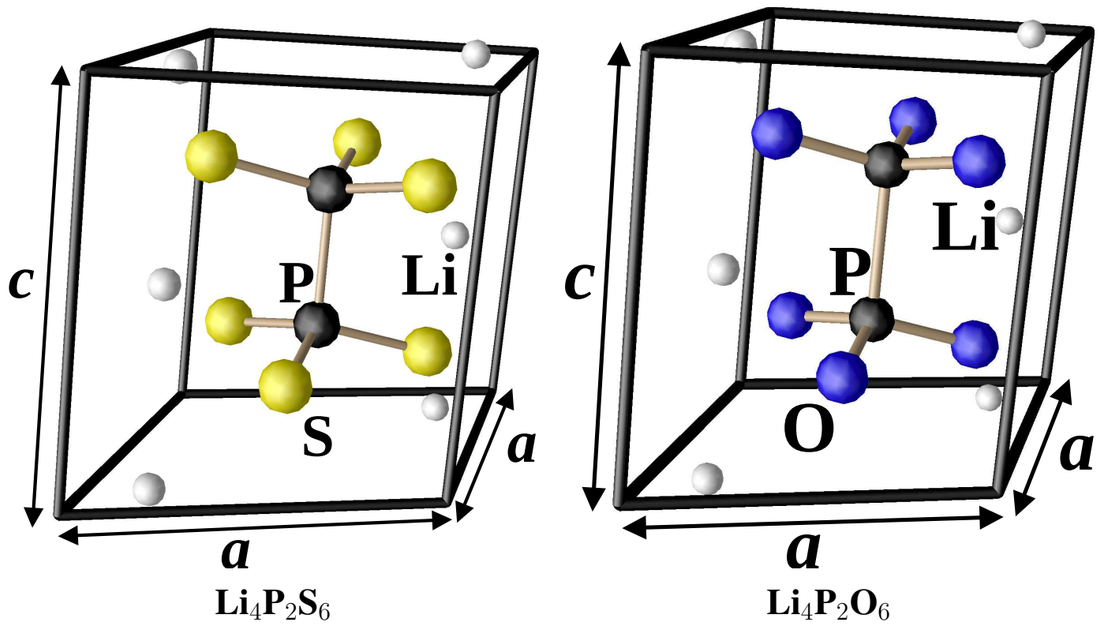

FIG. 5 Ball and stick diagrams for unit cells of $Li_4P_2S_6$ (left) and $Li_4P_2O_6$ (right) in the $P\bar{3}1m$ structure.

WAKE FOREST UNIVERSITY

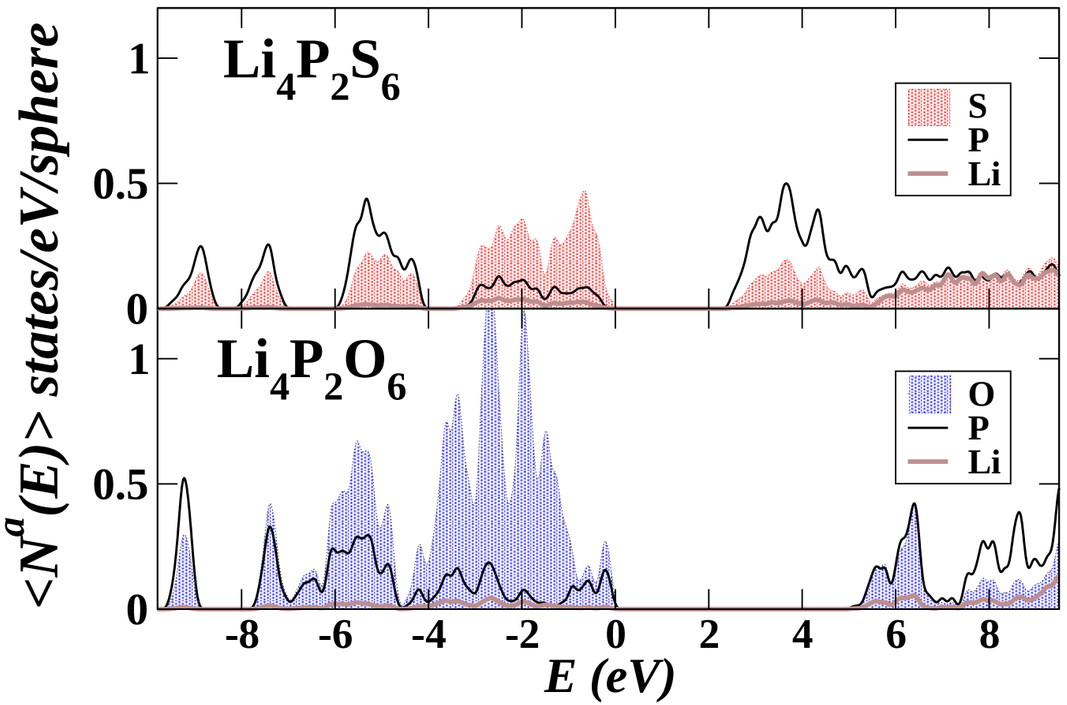

FIG.6 Partial densities of states for $Li_4P_2S_6$ and $Li_4P_2O_6$.

Partial densities of states for $Li_4P_2O_6$ and $Li_4P_2S_6$ are compared. In addition to the bands corresponding to S $3p$ states, one additional valence band is present due to the filled P $3s\sigma$ bond, whose contribution is concentrated near the bottom of the spectrum.

$Li_4P_2S_7$ and $Li_4P_2O_7$

While to the best of our knowledge, the crystal structure of $Li_4P_2S_7$ is unknown, $Li_4P_2O_7$ was found to crystallize[18] in the $P\bar{1}$ structure (#2). Our simulations confirm this structure and simulations for the corresponding thiophosphate – $Li_4P_2S_7$ – show that it has at least a meta-stable state in the same structure.

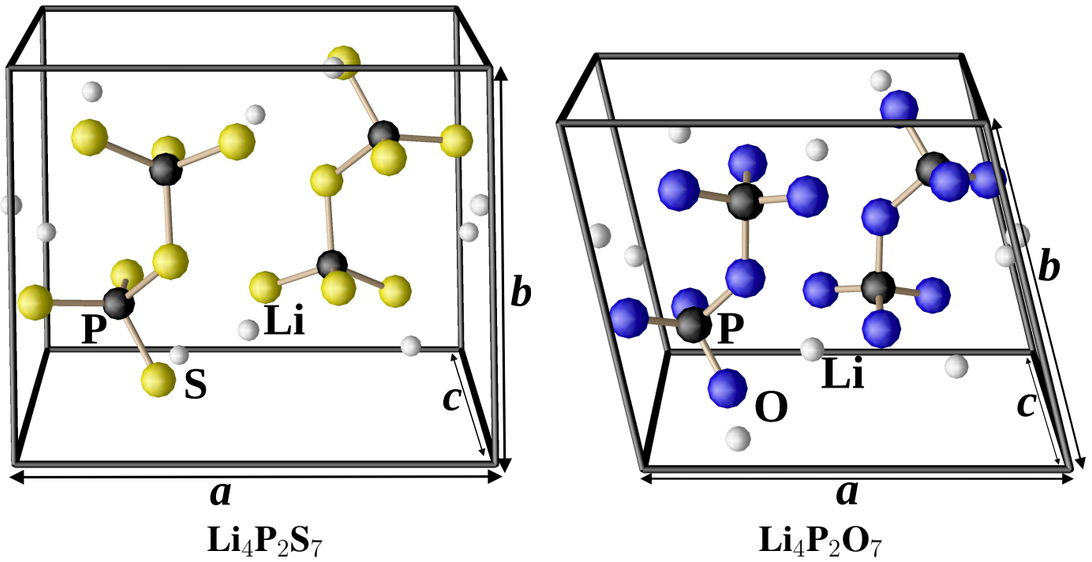

$Li_4P_2S_7$ $Li_4P_2O_7$

FIG. 7 Ball and stick diagrams for unit cells of $Li_4P_2S_7$ (left) and $Li_4P_2O_7$ (right) in the $P\bar{1}$ structure.

WAKE FOREST UNIVERSITY

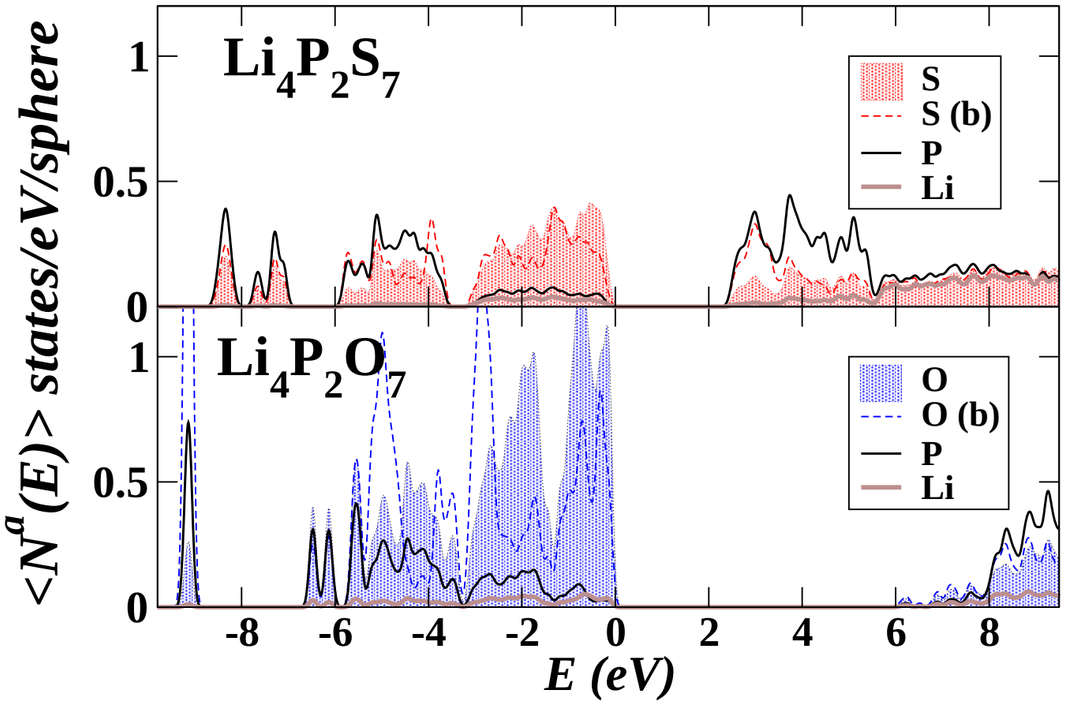

FIG.8 Partial densities of states for $Li_4P_2S_7$ and $Li_4P_2O_7$. Contributions from bridging S or O sites are indicated with "(b)".

Partial densities of states for $Li_4P_2O_7$ and $Li_4P_2S_7$ are compared. For these materials, while states with contributions from the P site contribute throughout the valence band, there is no additional valence state due to filled P states as in the case of $Li_4P_2O_6$ and $Li_4P_2S_6$. On the other hand there are two types of O (S) states. In addition to the normal tetrahedral O (S) site contributions, the "bridging" O (S) site contributions are shown separately on the plot. In particular, there is a band at the bottom of the valence band states which corresponds to states characterized primarily by O $2p\sigma$ or S $3p\sigma$ contributions for $Li_4P_2O_7$ and $Li_4P_2S_7$, respectively.

Heats of Formation

In order to assess the chemical stability of the materials, we estimated the heats of formation relative to their decomposition to elemental materials in their standard states as defined in the CRC Handbook,[19] using the methods described in our earlier work. In order to extend the analysis to sulfur containing materials we needed to estimate the equilibrium energy of the standard state of elemental S, which is the orthorhombic form (α-S_8)[20] having the structure $Fddd$ (#70). In order to extend the analysis to Cl-containing materials, we needed to estimate the energy of the standard state of elemental Cl, which is molecular Cl_2. Instead of evaluating this energy directly, we estimated it from the total energies of LiCl in the rocksalt structure, $LiClO_4$ in the $Pnma$ (#62) structure,[21] and PCl_5 in the $P4/n$ (#85) structure[22] and the heat of formation data values for these materials given in the CRC Handbook.

From these results, we can make some comments on relative stabilities of these materials. For example, the calculations suggest that $Li_4P_2S_6$ is more stable than $Li_4P_2S_7$ in the sense that in their standard states:

$$\Delta H(Li_4P_2S_6) + \Delta H(S) = \Delta H(Li_4P_2S_7) - 0.84\ \mathrm{eV}.$$

In fact there are literature reports of glassy $Li_4P_2S_7$, but we know of no reports of crystalline $Li_4P_2S_7$. By constrast, for the analogous phosphate materials, we find

$$\Delta H(Li_4P_2O_6) + \frac{1}{2}\Delta H(O_2) = \Delta H(Li_4P_2O_7) + 4.21\ \mathrm{eV},$$

suggesting that $Li_4P_2O_6$ is significantly unstable relative to $Li_4P_2O_7$. In fact we know of no literature reports of observations of $Li_4P_2O_6$ crystals. For the argyrodite material, the calculations also suggest that Li_7PS_6 is unstable relative to decomposition into Li_3PS_4 and Li_2S in the sense that

$$\Delta H(Li_7PS_6) = \Delta H(Li_3PS_4) + 2\Delta H(Li_2S) + 0.32\ \mathrm{eV}.$$

In this estimate, we used the β-Li_3PO_4 structure to evaluate $\Delta H(Li_3PS_4)$ and the result is within our expected calculation error. The material with chlorine is also marginally unstable relative to decomposition into Li_3PS_4, Li_2S , and LiCl as shown in the

$$\Delta H(Li_6PS_5Cl) = \Delta H(Li_3PS_4) + \Delta H(Li_2S) + \Delta H(LiCl) + 0.38\ \mathrm{eV}.$$

WAKE FOREST UNIVERSITY

TABLE I Heats of formation per formula unit calculated for the listed reference and lithium phosphate and thiophosphate materials. The structure is described in terms of the space group using the notation of The International Table of Crystallograph. When available, experimental values of ΔH from The CRC Handbook[19] are also listed.

Material	Structure	ΔH_{cal} (eV)	ΔH_{exp} (eV)
Li_2O	$Fm\bar{3}m$ (#225)	-6.13	-6.20
β-Li_3PO_4	$Pmn2_1$ (#31)	-21.31	
γ-Li_3PO_4	$Pnma$ (#62)	-21.28	-21.72
$Li_4P_2O_7$	$P\bar{1}$ (#2)	-34.10	
$Li_4P_2O_6$	$P\bar{3}1m$ (#162)	-29.89	
Li_2S	$Fm\bar{3}m$ (#225)	-4.26	-4.57
β-Li_3PS_4	$Pmn2_1$ (#31)	-8.32	
γ-Li_3PS_4	$Pnma$ (#62)	-8.12	
Li_7PS_6	$Pna2_1$ (#33)	-16.51	
$Li_4P_2S_7$	$P\bar{1}$ (#2)	-11.51	
$Li_4P_2S_6$	$P\bar{3}1m$ (#162)	-12.35	
$Li_7P_3S_{11}$	$P\bar{1}$ (#2)	-19.89	
LiCl	$Fm\bar{3}m$ (#225)	-3.80	-4.23
$LiClO_4$	$Pnma$ (#62)	-4.49	-3.95
PCl_5	$P4/n$ (#85)	-4.08	-4.60
Li_6PS_5Cl	Cc (#9)	-16.00	

The calculations also suggest that $Li_7P_3S_{11}$ is marginally stable with respect to decomposition into Li_3PS_4 and $Li_4P_2S_7$ in the sense that

$$\Delta H(Li_7P_3S_{11}) = \Delta H(Li_3PS_4) + \Delta H(Li_4P_2S_7) - 0.06\ \mathrm{eV}.$$

Again, this is within the expected calculational error.

Li Ion Migration Energies

An important question about these materials is how the Li ion migration differs in the phosphate and thiophosphate materials. A measure of the ionic conductivity σ as a function temperature T is expected to follow the Arrehenius relation:

$$\sigma \cdot T = K\ n\ \mathrm{e}^{-E_m/kT},$$

where k is the Boltzmann constant, K is a material-dependent parameter, n is the number of mobile Li ions or Li ion vacancies, and E_m is the migration energy.

In this initial study, we focus on the migration energy E_m for Li ion vacancy migration in idealized crystals of $Li_4P_2O_7$ and $Li_4P_2S_7$. These two materials form similar stable and meta-stable crystals with $P\bar{1}$ symmetry. For the simulations, we constructed $1 \times 2 \times 2$ supercells and studied the migration of a Li ion vacancy between 6 sites separated by roughly 3.0 Å and 3.6 Å for $Li_4P_2O_7$ and $Li_4P_2S_7$, respectively. The sites do not span a complete path within the supercell but do cover a representative range of crystal environments. The 6 sites are illustrated in Fig. 9 for the $Li_4P_2S_7$ supercell. A corresponding geometry was used for the $Li_4P_2O_7$ supercell.

The band occupancies of the supercell states were adjusted in order to approximate an insulating environment for ion migration, and the excess charge was compensated by adding a uniform charge of the opposite sign. The 6 optimized configurations for a Li ion vacancy were used as the end points for the NEB calculation in which 7 intermediate images were used to approximate the minimum energy path. The energy path diagram is shown in Fig. 9, comparing the results for $Li_4P_2S_7$ and $Li_4P_2O_7$.

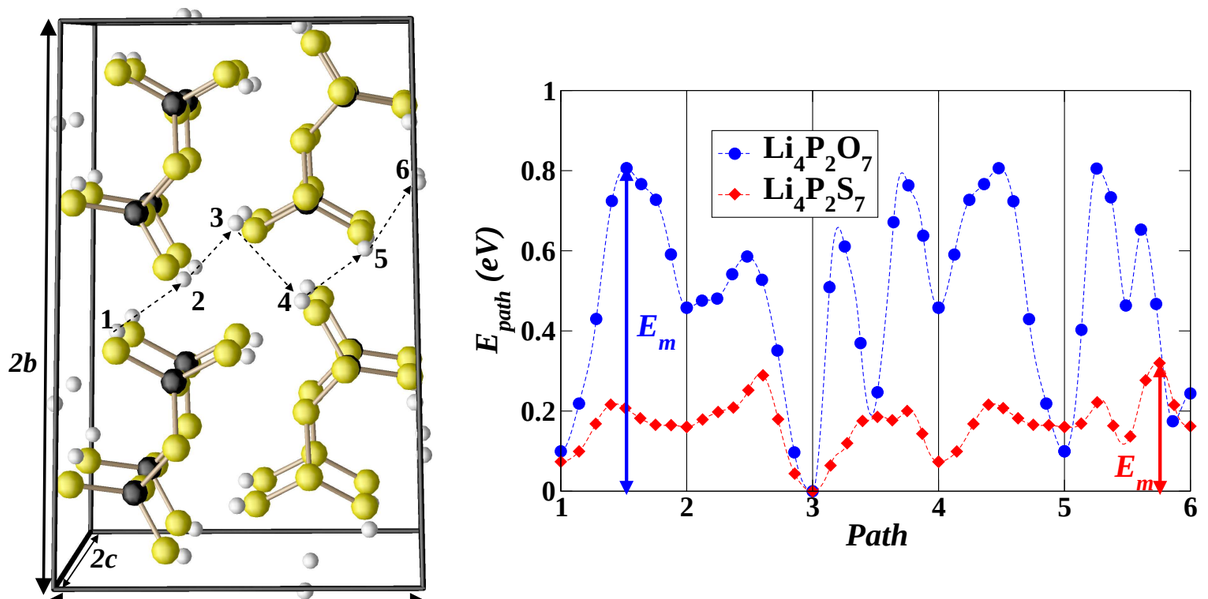

FIG. 9 Left: Li ion vacancy sites used in migration energy study in $Li_4P_2S_7$. Similar sites were used for $Li_4P_2O_7$. Right: Energy path diagram for Li ion vacancy migration in $Li_4P_2S_7$ and $Li_4P_2O_7$. The integer labels on the the horizontal axis correspond to the 6 vacancy sites indicated in the structural diagram. Between each pair of optimized vacancy configurations are 7 NEB image configurations along the minimum energy path. The continuous line is constructed with a spline interpolation between the image energies.

As is evident from the energy path diagram shown in Fig. 9 , the energy landscape for this system is complicated. However, the results indicate a clear qualitative result that the migration energy barriers for Li ion vacancy migration in $Li_4P_2S_7$ is less than half that in $Li_4P_2O_7$. For the particular migration path chosen, we find the migration energy energy barriers to be E_m = 0.3 eV for $Li_4P_2S_7$ and E_m = 0.8 eV for $Li_4P_2O_7$.

Summary and Conclusions

This study has found some interesting similarities and differences between the phosphate and thiophosphate materials. Our structural optimizations were generally in good agreement with the experimental structures, although there are some differences. For example, our calculations for Li_3PS_4 indicated that the most stable structure is that of β-Li_3PO_4, while the experiment[14] indicated a structure similar to γ-Li_3PO_4 with partial occupancies of some of the sites. A similar discrepancy was found for the structure of $Li_4P_2S_6$.[17] These differences are undoubtedly related to real temperture effects which are not considered in the simulations.

In general, a greater variety in the bonding configurations of the thiophosphates is observed compared with those of the phosphates. The argyrodite structures[15] with unbounded S and Cl groups within the crystal and increased concentrations of Li ions are very intriguing.

In addition to our analysis of the optimized structures and their stabilities, we have presented some preliminary results pertaining to Li ion vacancy migration within a representative set of materials. We find that the energy barriers for Li ion vacancy migration in $Li_4P_2S_7$ to be less than half that for $Li_4P_2O_7$. This result is consistent with the experimental observation of increased ionic conductivity in the thiophosphate materials compared with those of the phosphates. Our analysis suggests that one factor contributing to the lowered potential barriers in the thiophosphates is the more diffuse valence charge distribution near the S sites compared with the compact valence charge distribution near the O sites.

Acknowledgements

This work was supported by NSF grants DMR-0427055 and 0705239 and by the Wake Forest University DEAC computer cluster. We would like to thank Dr. F. Stadler for informing us about the argyrodite materials.

Bibliography

[1] J. B. Bates, et al., *Solid State Ionics* **5356**, 647 (1992); N. J. Dudney, *Interface* **17** (3), 44 (2008).

[2] Y. A. Du, N. A. W. Holzwarth, *Journal of the Electrochemical Society* **154**, A999 (2007); Y. A. Du, N. A. W. Holzwarth, *Phys. Rev. B* **81**, 184106 (15pp) (2010).

[3] F. Mizuno, A. Hayashi, K. Tadanaga, M. Tatsumisago, Electrochemical and Solid- State Letters **8**, A603 (2005); K. Minami, A. Hayashi, M. Tatsumisago, *Solid State Ionics* **179**, 1282 (2008); A. Hayashi, K. Minami, M. Tatsumisago, Journal of Non-crystalline Solids **355**, 1919 (2009); J. Trevey, J. S. Jang, Y. W. Jung, C. R. Stoldt, S.-H. Lee, Electrochemistry Communications **11**, 1830 (2009).

[4] P. Hohenberg, W. Kohn, *Physical Review* **136**, B864 (1964); W. Kohn, L. J. Sham, *Physical Review* **140**, A1133 (1965).

[5] J. P. Perdew, Y. Wang, *Phys. Rev. B* **45**, 13244 (1992).

[6] P. Giannozzi, et al., *J. Phys.: Condens. Matter* **21**, 394402 (19pp) (2009). Available from the website `http://www.quantum-espresso.org`.

[7] X. Gonze, et al., Zeit. Kristallogr. **220**, 558 (2005). Available from the website `http://www.abinit.org`.

[8] A. R. Tackett, N. A. W. Holzwarth, G. E. Matthews, *Computer Physics Communications* **135**, 348 (2001). Available from the website `http://pwpaw.wfu.edu`.

[9] OpenDX The Open Source Software Project Based on IBMs Visualization Data Explorer is available from the web site `http://www.opendx.org`.

[10] A. Kokalj, *Journal of Molecular Graphics and Modelling* **17**, 176 (1999).

[11] H. Jónsson, G. Mills, K. W. Jacobsen, *Classical and Quantum Dynamics in Condensed Phase Simulations*, B. J. Berne, G. Ciccotti, D. F. Coker, eds. (World Scientific, Singapore, 1998), pp. 385404; G. Henkelman, B. P. Uberuaga, H. Jónsson, *J. Chem. Phys.* **113**, 9901 (2000); G. Henkelman, H. Jónsson, *J. Chem. Phys.* **113**, 9978 (2000).

[12] C. Keffer, A. Mighell, F. Mauer, H. Swanson, S. Block, *Inorganic Chemistry* **6**, 119 (1967).

[13] O. V. Yakubovich, V. S. Urusov, *Crystallography Reports* **42**, 261 (1997).

[14] R. Mercier, J.-P. Malugani, B. Fahyst, G. Robert, *Acta Cryst. B* **38**, 1887 (1982).

[15] S. T. Kong, et al., *Chem. Eur. J.* **16**, 5138 (2010); S. T. Kong, et al., *Chem. Eur. J.* **16**, 2198 (2010); H.-J. Deiseroth, et al., *Angew. Chem. Int. Ed.* **47**, 755 (2008).

[16] F. Stadler, C. Fietzek, ECS Trans. **25**, 177 (2010).

[17] R. Mercier, J. P. Malugani, B. Fays, J. Douglade, G. Robert, *Journal of Solid State Chemistry* **43**, 151 (1982).

[18] A. Daidouh, M. L. Veiga, C. Pico, M. Martinez-Ripoll, *Acta Cryst. C* **53**, 167 (1997).

[19] D. R. Lide, ed., *CRC Handbook of Chemistry and Physics*, 90th Edition (CRC Press, Taylor & Francis Group, 2009). ISBN 13: 978-1-4200-9084-0.

[20] S. J. Rettig, J. Trotter, *Acta Cryst. C* **43**, 2260 (1987).

[21] K. D. M. Harris, M. Tremayne, *Chem. Mater.* **8**, 2554 (1996).

[22] D. Clark, H. M. Powell, A. F.Wells, *Journal of the Chemical Society* **134**, 642 (1942).